Int. J. Electrochem. Sci., 17 **(2022)** Article Number: 220131, doi: 10.20964/2022.01.18

International Journal of
ELECTROCHEMICAL
SCIENCE
www.electrochemsci.org

Corrosion Behaviour of 1018 Carbon Steel in LiBr-H_2O-$CaCl_2$-$LiNO_3$ Mixtures

A.K. Larios-Galvez[1], R. Guardian-Tapia[1], R. Lopez-Sesenes[2], J.G. Gonzalez-Rodriguez[1],*

[1] Universidad Autonoma del Estado de Morelos, Centro de Investigación en Ingeniería y Ciencias Aplicadas, Av.Universidad 1001, 62209-Cuernavaca, Morelos, Mexico
[2] Universidad Autonoma del Estado de Morelos, Facultad de Ciencias Quimicas e Ingenieria, Av.Universidad 1001, 62209-Cuernavaca, Morelos, Mexico
[*]E-mail: ggonzalez@uaem.mx

Received: 5 October 2021 / *Accepted:* 1 November 2021 / *Published:* 6 December 2021

A study on the effect of $CaCl_2$, $LiNO_3$ and $CaCl_2$+$LiNO_3$ to the LiBr-H_2O system on the corrosion behaviour of 1018 carbon steel was performed with the aid of electrochemical techniques such as potentiodynamic polarization curves and electrochemical impedance spectroscopy. This system is used in conventional refrigeration absorption systems. LiBr was used at different concentrations (283.3, 425 and 825 g/L) and temperatures (25, 50 and 80°C). Corrosion current density value, I_{corr}, obtained in the LiBr+H_2O system decreased with the addition of these additives, obtaining the lowest value when $CaCl_2$ was added. I_{corr} values increased with both an increase in the testing temperature and the LiBr concentration. In addition to this, corrosion process for the LiBr-H_2O system was under desorption/desorption control, whereas in presence of these additives it was either under charge transfer or reactants diffusion control depending upon the testing temperature or LiBr concentration.

Keywords: Absorption systems; corrosion; carbon steel.

1. INTRODUCTION

Conventional, refrigeration absorption systems which operate by mechanical compression use chlorofluorocarbon compounds which are dangerous for the ozone layer when they are exposed to the atmosphere [1,2], and for this reason, new adsorption systems either work with solar energy or use waste heat and use refrigerant compounds that do not cause any damage to the environment [3-9]. LiBr-H_2O is the most widely used working fluid in the adsorption systems due to their thermophysical properties [10], where H_2O is the refrigerant and LiBr the absorbent ; however, this working system produces high crystallization temperature [11-13] and corrosion problems with the metallic components, for instance,

for the ferrous alloys such as carbon steel [14, 15], stainless steel [16, 17] and non-ferrous materials such as nickel [18], and cooper and its alloys [19, 20]. Due to its low cost, carbon steel is widely used in some metallic components in the adsorption cooling systems, however, it is very susceptible to corrosion problems in the $LiBr+H_2O$ working fluids [14, 15]. Therefore, many research works are currently carried out with different working fluids used in refrigeration systems to find solutions to the problems associated to corrosion, solubility, crystallization temperature, vapour pressure, chemical and thermal stability, among others. Thus, Li proposed as absorber a ternary mixture, $CaCl_2+LiBr+LiNO_3$, for an adsorption system based on one step that uses solar energy [21], whereas Li carried out a study by using the de $CaCl_2+LiNO_3+KNO_3+H_2O$ quaternary system [22], showing, in both studies, a decrease in the vapour pressure and in the crystallization temperature. Torres [23] analysed the efficiency of an adsorption thermal transformer by using as absorber a quaternary mixture which included $LiBr+LiI+LiNO_3+LiCl+H_2O$, where the addition of Li salts improved the LiBr solubility. Bellos [24] and Luo [25] evaluated the $LiCl+H_2O$ and $LiNO_3+H_2O$ binary salts as working fluids in the adsorption refrigerating system, finding a better efficiency with the presence of LiCl whereas the presence of $LiNO_3$ decreased the system corrosion rate. In addition to this, working fluids containing organic compounds such as LiBr+1-etil-3-methylimidazolium (EMIM)$Cl+H_2O$. The presence of [EMIM]Cl decreased the crystallization temperature whereas the vapour pressure was similar to that found for the $LiBr+H_2O$ system [26]. Thus, this research work focus on the corrosion behaviour of 1018 carbon steel in the $CaCl_2+LiBr+LiNO_3+H_2O$ system at different testing temperatures and concentrations.

2. EXPERIMENTAL PROCEDURE

2.1. Testing material

Material used in this research work included a 6.0 mm diameter rode 1018 carbon steel containing (wt. %) 0.14% C, 0.90% Mn, 0.03% P and balance Fe. Specimens were encapsulated in a polymeric resin, polished using silicon-carbide paper 600 grade. The samples were finally washed with acetone and then distilled water before use.

2.2. Testing solutions

Tests were carried out using $LiBr+H_2O$ as base solution in concentrations of 850, 425 and 283.3 g/L [27] to see the effect of solution concentration. In order to see the individual effect of $CaCl_2$ and $LiNO_3$ salts, some tests were in solutions containing mixtures of $CaCl_2+LiBr(1.35:1) + H_2O$, [21,22] $LiBr+LiNO_3$ (4:1) $+H_2O$. [28] Finally, in order to see the combined effect of $CaCl_2$ and $LiNO_3$, a solution containing $CaCl_2+LiBr+LiNO_3$ (8.72:1:1)$+H_2O$ [29] was evaluated. When the concentration of LiBr was changed, the $CaCl_2$/LiBr, $LiNO_3$/LiBr and $CaCl_2$-LiBr-$LiNO_3$ ratios were kept at 1.35:1, 4:1 and 8.72:1:1 respectively. All these tests were carried out at 80°C. Finally, in order to see the effect of temperature, solution containing $CaCl_2+LiNO_3+LiBr +H_2O$ containing 850 g/L LiBr were evaluated at 25 and 50 °C.

2.3. Electrochemical techniques

Electrochemical techniques used in the present research work includes potentiodynamic polarization curves and electrochemical impedance spectroscopy (EIS). To achieve this, a three electrodes cell was used, using graphite rode as auxiliary electrode, whereas a silver/silver chloride (Ag/AgCl) electrode was used as reference. Before starting the tests, the open circuit potential value (OCP) was monitored and waited until it reached a stable value. Potentiodynamic polarization curves started at a potential value 600 mV more negative than the free corrosion potential value, E_{corr}, and ending at 1,200 mV more anodic than E_{corr} at a sweep rate of 60 mV/min. Corrosion current density values, I_{corr}, was calculated with the aid of the Tafel extrapolation technique. Finally, EIS experiments were carried out at the E_{corr} value by polarizing the specimens ± 10 mV in the frequency interval of 0.01-100 KHz by using Gill AC Serial 1340-Sequencer. Selected specimens were analysed in a low vacuum LEO 1450VP scanning electronic microscope (SEM) after being corroded.

3. RESULTS AND DISCUSSION

3.1 Open circuit potential

The effect of testing temperature on the variation of the open circuit potential value (OCP) with time for the different mixtures containing 850 g/L LiBr is given in Fig. 1. At 25 °C, Fig. 1 a, it can be seen that the OCP value for the base LiBr+H_2O solution rapidly shifts towards more active values, indicative of the dissolution of any pre-formed corrosion products layer on the steel surface [30].

The same trend had the OCP values for solutions when either $CaCl_2$ or $LiNO_3$ were added, although the value observed for the later was more active, whereas that observed for the former was nobler. However, when both $CaCl_2$ and $LiNO_3$ were added, the observed OCP value was the noblest, indicating the formation of a more protective corrosion products layer onto the steel surface [30].

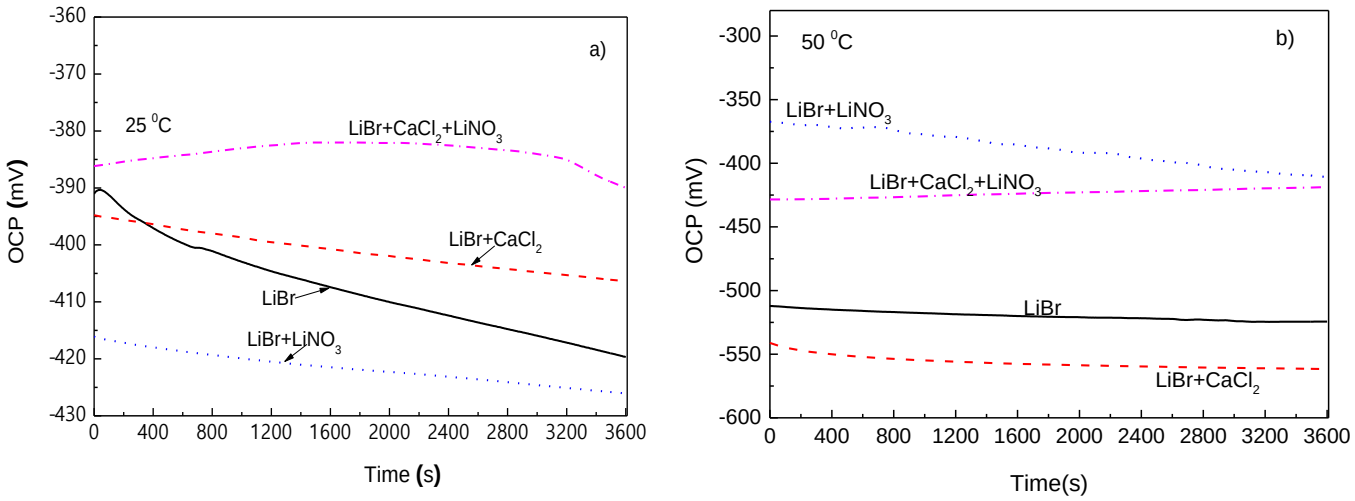

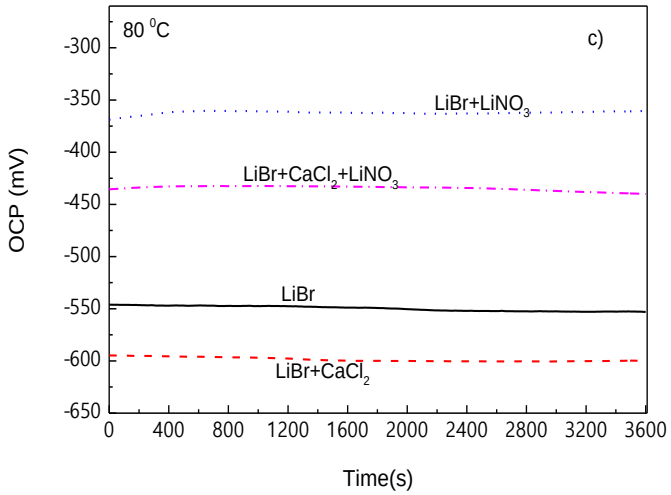

Figure 1. Effect of the addition of $CaCl_2$ and $LiNO_3$ to LiBr/H2O (850 g/L) on the OCP value for 1018 carbon steel at a) 25, b) 50 and c) 80 °C.

When the testing temperature increased up to 50 °C, Fig. 1 b, all the OCP values remained relatively constant with time, but they were more active than those observed at 25°C, indicating a higher tendency of the metal to be corroded. This time, the most active OCP value was observed for the solution containing $CaCl_2$, whereas the noblest value was observed in the solutions containing either only $LiNO_3$ although after 3600 s of testing its value was very close to that observed in the solution containing $CaCl_2$+$LiNO_3$. When the temperature reached 80°C, Fig. 1 c, the OCP values became even more active than those observed at 50 and 25°C, remaining very stable as time elapsed. Once again, the most active OCP value was observed for the solution containing $CaCl_2$, whereas the noblest one was observed for the solution containing $LiNO_3$. Thus, it is clear that an increase in the testing temperature made the OCP values to become more actives, whereas, at least at 50 and 80 °C, the addition of $CaCl_2$ to the LiBr+H_2O mixture made the OCP value more active, whereas the addition of $LiNO_3$ made this value to become nobler. The addition of both $CaCl_2$+$LiNO_3$ to the LiBr+H_2O mixture made the OCP value nobler than that obtained in this mixture but slightly more active than obtained with the addition of $LiNO_3$ at least at 50 and 80 °C.

The OCP values at the LiBr concentrations of 283.3 and 425 g/L at 80°C are shown in Fig. 2. As compared to the OCP value obtained for pure LiBr+H_2O at a concentration of 850 g/L, it was virtually unaffected by the change in its concentration, since in all cases it fluctuated around a value of -550 mV, and kept that value during the rest of the experiment. The addition of either $LiNO_3$ alone to the LiBr+H_2O mixture shifted the OCP values towards nobler values at both LiBr concentrations, whereas the addition of $CaCl_2$ shifted it towards more active values.

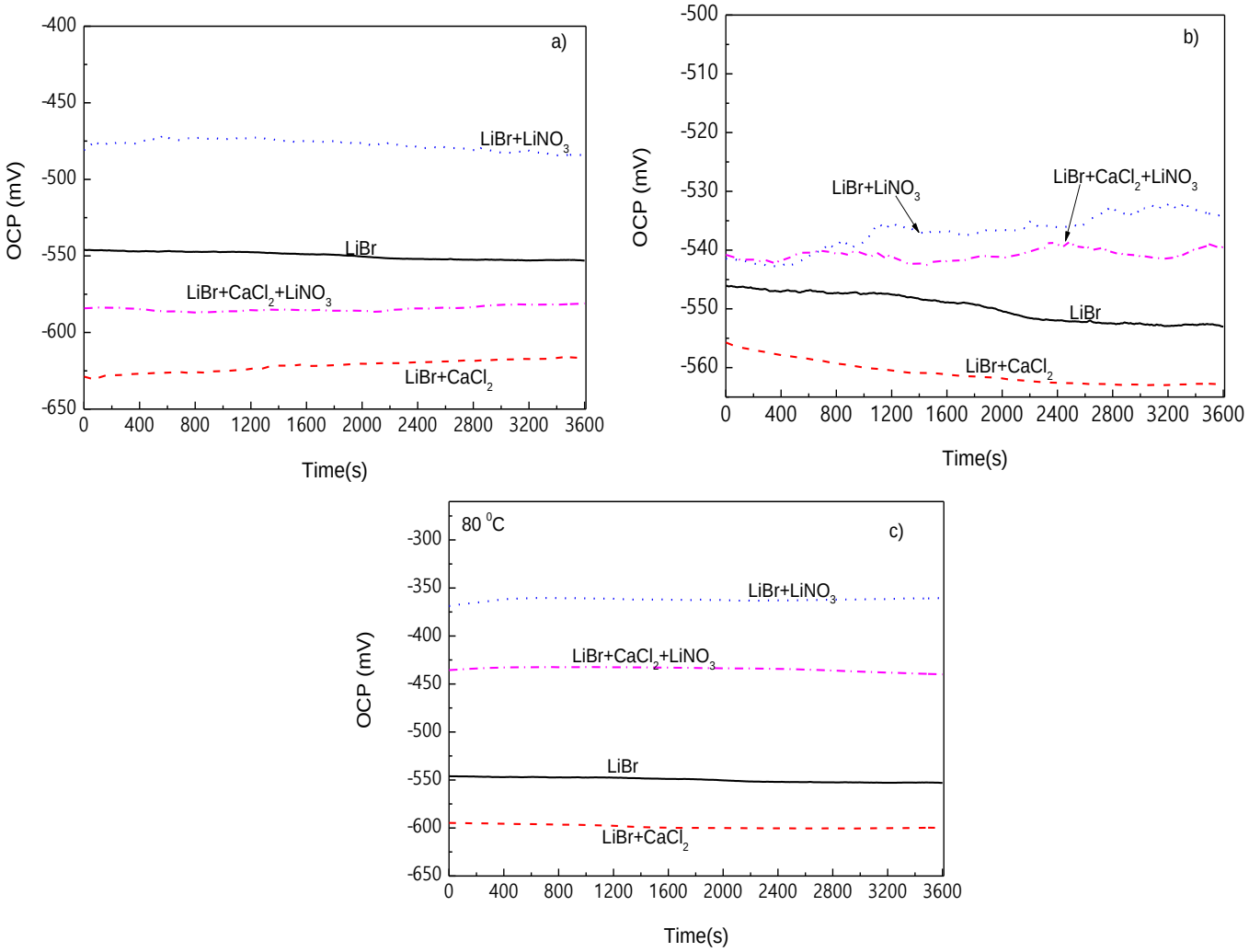

Figure 2. Effect of the addition of $CaCl_2$ and LiNO3 to $LiBr/H_2O$ on the OCP value for 1018 carbon steel at a LiBr concentration of a) 283.3, b) 425 and c) 850 g/L at 80 °C.

3.2 Polarization curves

The effect of the addition of $CaCl_2$, $LiNO_3$ and $CaCl_2$+$LiNO_3$ to the LiBr+ H_2O solution on the polarization curves of carbon steel at different testing temperatures is shown in Fig. 3. At 25 °C, Fig. 3 a, data for the LiBr+H_2O solution displayed an active-passive behaviour, with a wide passive zone which extends from a potential value of -800 mV and ends at a potential value close to -410 mV. This passive layer has been reported by Liang [31] as well as by Hu [32] to be due to the formation of a layer of Fe_2O_3 on top of steel surface. Passive current density value, Ipas, was around 20 $\mu A/cm^2$, similar to the value obtained by Hu for carbon steel in 55% LiBr+ 0.07 mol/L LiOH solution, who found an I_{pas} value of 15 $\mu A/cm^2$ [32]. On the other hand, Liang [31] found that, in addition to the Fe_2O_3 film formed on top of carbon, the presence of Fe_3O_4 was also noticed, being the dominant the former. The formation of Fe_3O_4 was explained as follows:

Anodic reaction:

$$3\ Fe \rightarrow 3\ Fe^{2+} + 6e \quad (1)$$

$$2Fe+6OH^- \rightarrow Fe_2O_3 + 3H_2O + 6e \quad (2)$$

Cathodic reaction:

$$2H_2O + 2e \rightarrow 2OH^- + H_2 \quad (3)$$

whereas the formation of Fe_3O_4 was explained according to:

$$Fe^{2+} + H_2O \rightarrow FeOH^+ + H^+ \quad (4)$$

$$3FeOH^+ + H_2O \rightarrow Fe_3O_4 + 5H^+ + 2e \quad (5)$$

$$2H^+ + e \rightarrow H_2 \quad (6)$$

The addition of either $CaCl_2$, $LiNO_3$ or $CaCl_2$+$LiNO_3$ to the LiBr+H_2O solution did not affect the active-passive behaviour, since in all cases a passive zone was present in the polarization curves.

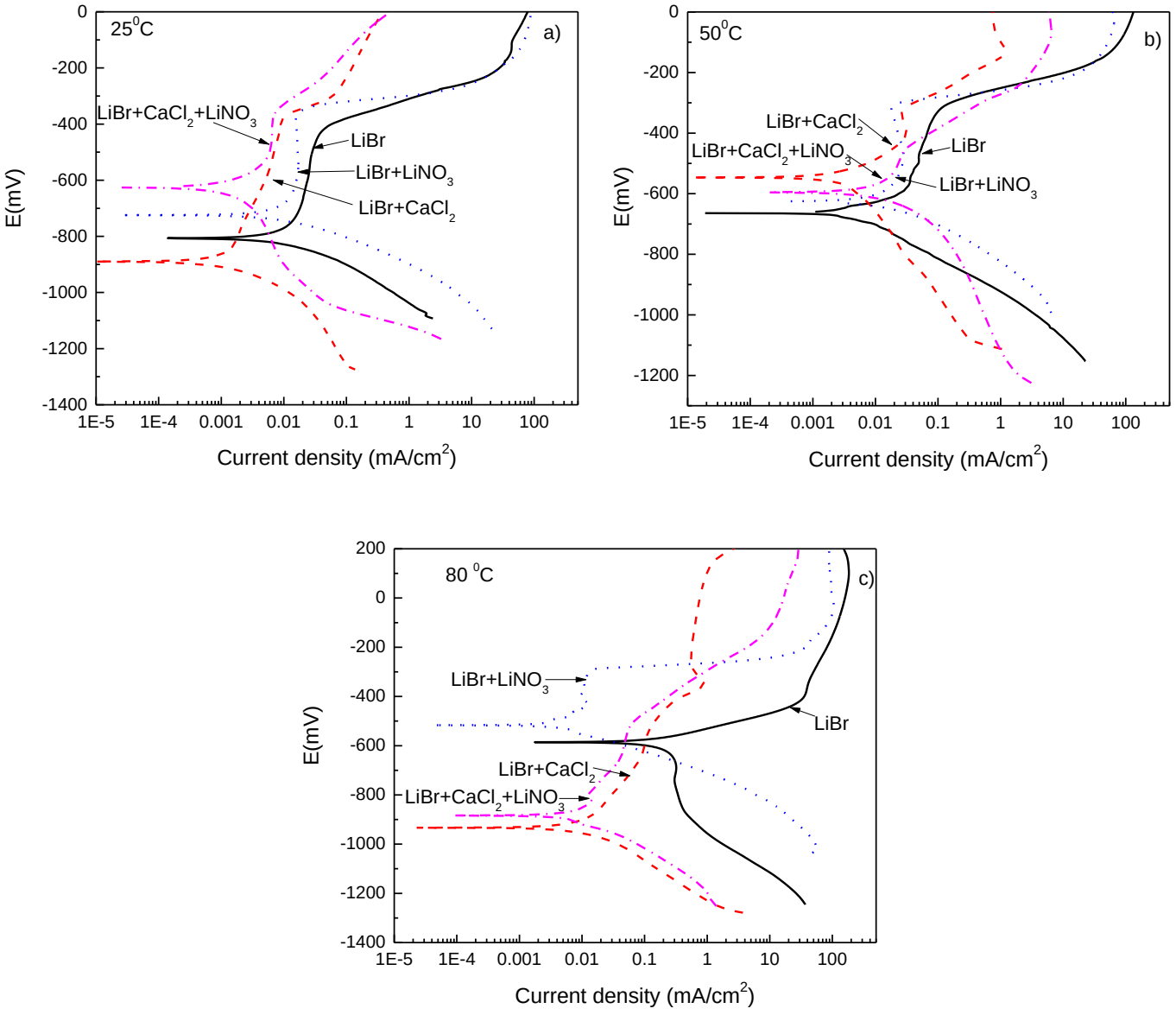

Figure 3. Effect of the addition of $CaCl_2$ and $LiNO_3$ to LiBr/H_2O (850 g/L) on the polarization curves for 1018 carbon steel at a) 25, b) 50 and c) 80 °C.

The addition of $LiNO_3$ decreased the I_{corr} value obtained in the $LiBr+H_2O$ solution, since it is very well known the fact that $LiNO_3$ forms a protective film [25, 28, 29] For instance, Sarmiento-Bustos [33] working with 1018 carbon steel in the LiBr + ethylene glycol + H_2O mixture, found that polarization curve in absence of $LiNO_3$ displayed an active behaviour only, whereas with the addition of 5 ppm of $LiNO_3$, the presence of a passive zone was evident. Similarly, the addition of $CaCl_2+LiNO_3$ brought a decrease in the I_{corr} value, lower than that obtained with the addition of $LiNO_3$, however, the lowest I_{corr} value was obtained with the addition of $CaCl_2$. It is well known that $CaCl_2$ is highly corrosive to most of metals, including carbon steel and stainless steels [34, 35]. Ren found that corrosion rate for carbon steel in $CaCl_2$ solution increased with the temperature from 30 to 80° but it decreased with time due to the formation of a passive film. Similarly, Itoh [36] found that corrosion rate of carbon steel in concentrated $LiBr+CaCl_2$ mixed solution decreased with time due to the formation of a thick layer of corrosion products film on top of steel. Important to notice that the pitting potential value, E_{pit}, for the $LiBr+H_2O$ mixture was slightly increased with the addition of either $CaCl_2$, $LiNO_3$ or $CaCl_2+LiNO_3$. The passive behaviour displayed by polarization curves was maintained in all cases at 50°C, as shown in Fig. 3 b.

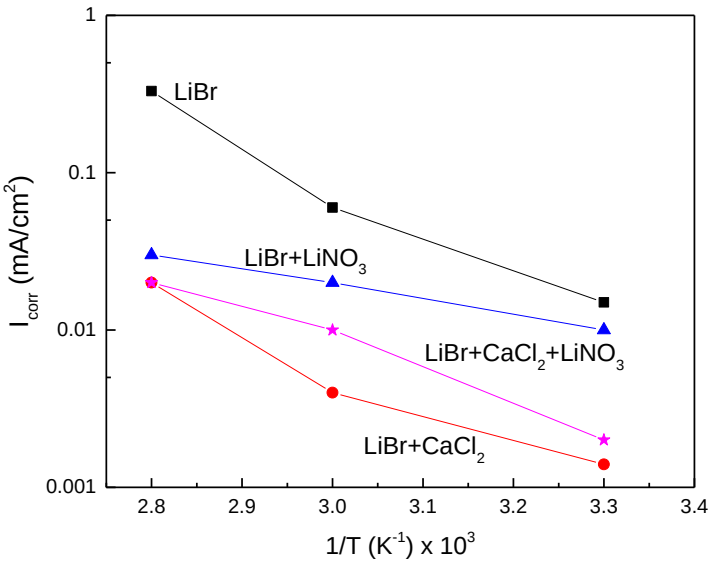

Figure 4. Arrhenius type of plot for the I_{corr} value of 1018 carbon steel immersed in $LiBr/H_2O$ containing $CaCl_2$ and $LiNO_3$.

The highest I_{corr} value was obtained in the $LiBr+H_2O$ mixture, but it was lowered with the addition of $LiNO_3$; the lowest one was obtained with the addition of $LiCl_2$. When the testing temperature reached 80°C, Fig. 3 c, there was no evidence of a passive layer on the polarization curve for the $LiBr+H_2O$ mixture but only anodic dissolution. However, polarization curves for the addition of $CaCl_2$, $LiNO_3$ and $CaCl_2+LiNO_3$ displayed an active-passive behaviour. However, the passive zone observed for the addition of $LiNO_3$ to the $LiBr+H_2O$ mixture was narrower than that obtained for addition of either $CaCl_2$ or $CaCl_2+LiNO_3$. The addition of either $CaCl_2$, $LiNO_3$ or $CaCl_2+LiNO_3$ decreased the I_{corr} value

obtained in the LiBr+H_2O mixture, obtaining the lowest value when $CaCl_2$ was added in to the system for nearly two orders of magnitude.

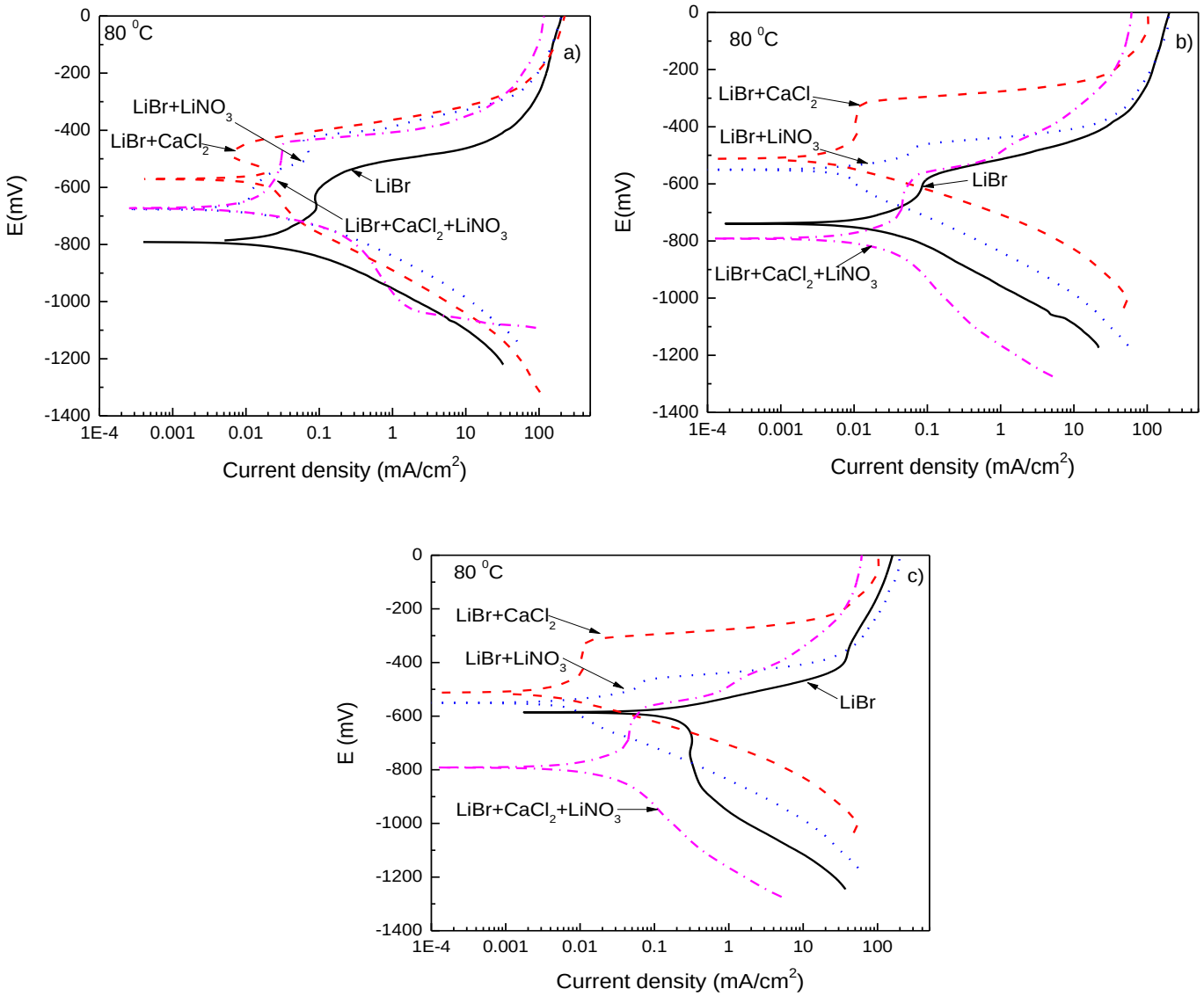

Figure 5. Effect of the addition of $CaCl_2$ and $LiNO_3$ to LiBr/H_2O on the polarization curves for 1018 carbon steel at a LiBr concentration of a) 283.3, b) 425 and c) 850 g/L at 80 °C.

An Arrhenius type of plot for the I_{corr} value for the different systems is given in Fig. 4 indicating an increase in the I_{corr} value with an increase in the testing temperature. With an increase in the testing temperature, molecules can collide more frequently and with more energy which increases the corrosion rate [37]. Similar plots for I_{corr} values obtained for carbon steels in LiBr solutions have been reported previously. For instance, Guiñon [38] found a similar trend between when plotted I_{corr}-vs-1/T for 1015 carbon steel in 400 g/L of LiBr+H_2O solution in a temperature interval between 25 and 80 °C. Similar trend was reported for nickel-base alloys and Alloy 900-type stainless steel in a solution containing 992 g/L LiBr+H_2O in the temperature interval between 25-80°C [18]. It is clear that with an increase in the

testing temperature, the I_{corr} values increased for all the different systems which may be to an increase in the aggressiveness of Br^- and the loss of protectiveness given by passive film [5, 18, 38]. However, this effect is less pronounced for I_{corr} values obtained when $LiNO_3$ was added to the $LiBr+H_2O$ mixture. The highest obtained I_{corr} value, was in the $LiBr+H_2O$ mixture, whereas the lowest value was obtained when $CaCl_2$ was added to the $LiBr+H_2O$ mixture.

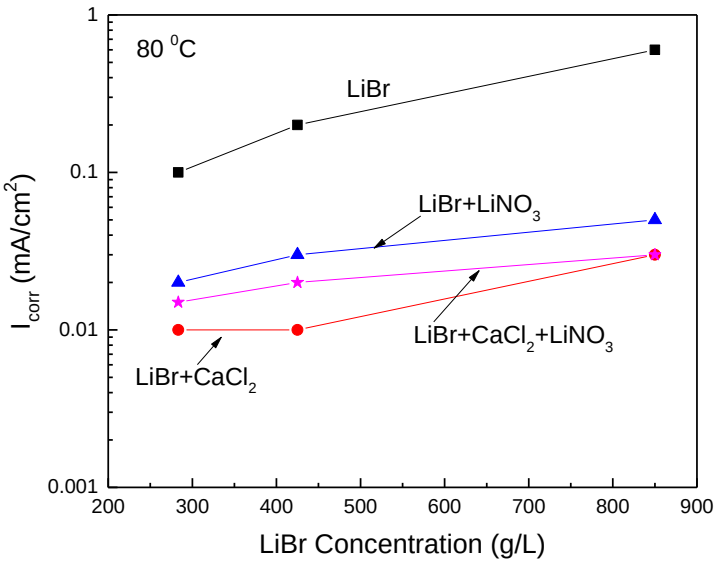

Figure 6. Effect of the addition of $CaCl_2$ and $LiNO_3$ to $LiBr/H_2O$ on the I_{corr} value for 1018 carbon steel at different LiBr concentrations.

Polarization curves for 1018 carbon steel in the $LiBr+H_2O$ mixture at different LiBr concentrations and with the addition of $LiNO_3$, $CaCl_2$ and $CaCl_2+LiNO_3$ at 80° C are shown in Fig. 5. We want to make emphasis that in these solutions, the $CaCl_2$/LiBr, $LiNO_3$/LiBr and $CaCl_2$-LiBr-$LiNO_3$ ratios were kept at 1.35:1, 4:1 and 8.72:1:1 respectively. It can be seen that for the LiBr+H2O mixture, data displayed an active-passive behaviour at low LiBr concentrations except at the highest LiBr concentration, where polarization curve did not show an active-passive behaviour, only an active behaviour. The passive zone exhibited by carbon steel became narrower as the LiBr concentration increased until this passive zone was absent at the most concentrated LiBr solution. Regardless the LiBr concentration, the addition of either $LiNO_3$ or $CaCl_2$ or their combination to the $LiBr+H_2O$ mixture kept the passive behaviour of carbon steel and decreased the I_{corr} value, obtaining the lowest value when $CaCl_2$ alone was added. A plot of I_{corr} versus LiBr concentration without and with the addition of either $LiNO_3$ or $CaCl_2$ or their combination is shown in Fig. 6, where it can be seen that, generally speaking, the I_{corr} value increased with an increase in the LiBr concentration. Guiñon [18] found a similar trend for 1015 carbon steel in $LiBr+H_2O$ by changing the LiBr concentration from 100 to 700 g/L at 80 °C. They reported that the LiBr concentration did not affect the I_{corr} value for pure Ti, but it had a similar effect for 4145 low alloy high strength steel, whereas the effect was more pronounced for 316 type stainless steel.

3.3 Electrochemical impedance spectroscopy.

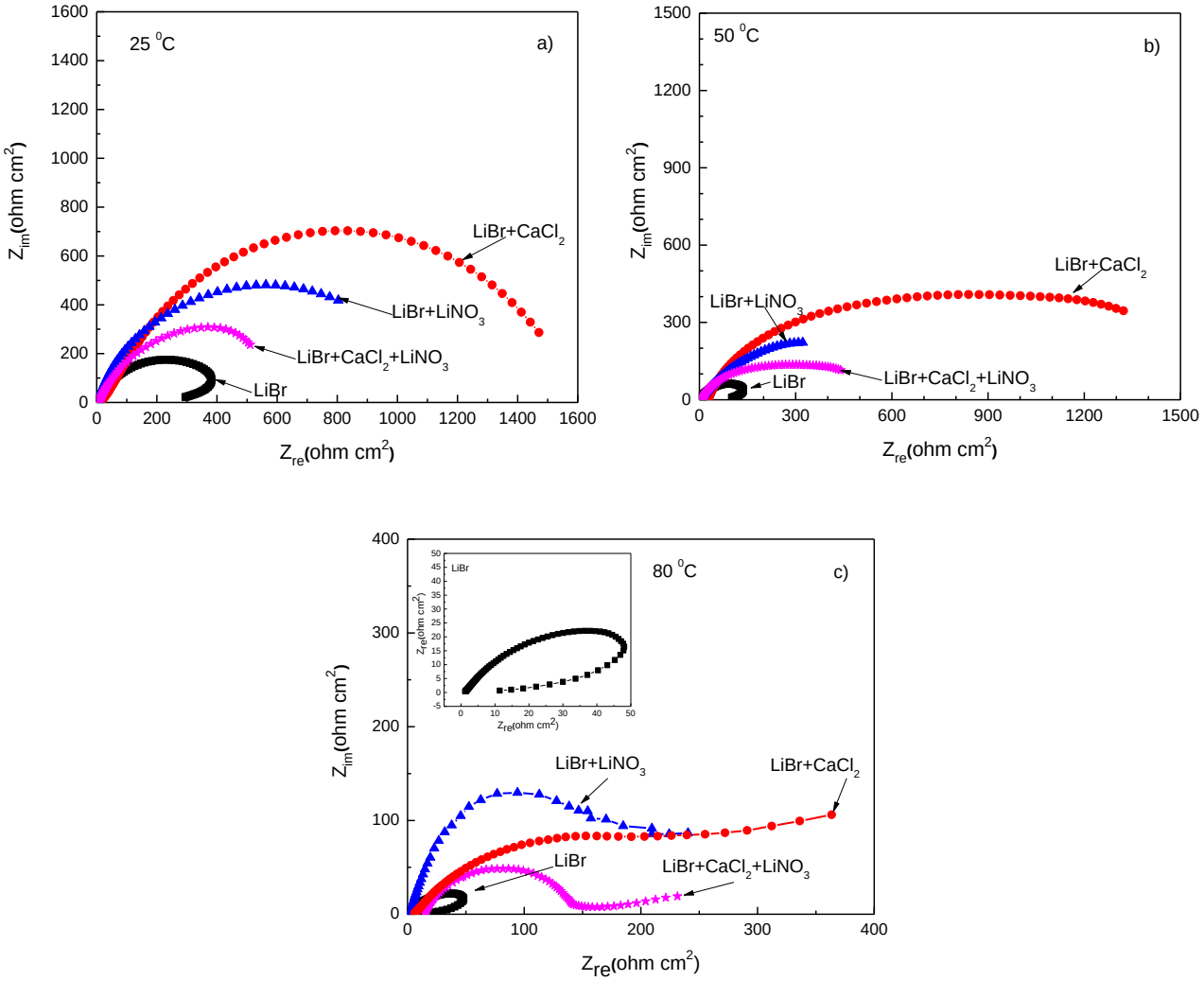

Figure 7. Effect of the addition of $CaCl_2$ and $LiNO_3$ to $LiBr/H_2O$ (850 g/L) on the Nyquist diagrams for 1018 carbon steel at a) 25, b) 50 and c) 80 °C.

The effect of the addition of $CaCl_2$, $LiNO_3$ and $CaCl_2$+$LiNO_3$ to the $LiBr+H_2O$ solution on the Nyquist plots of carbon steel at different testing temperatures is shown in Fig. 7. It can be seen that at regardless the temperature, a capacitive loop was observed in the Nyquist plots in the $LiBr+H_2O$ solution at high and intermediate frequencies, whereas at the lowest frequency values, an inductive semicircle could be seen, indicating that the corrosion process controlled by the adsorption/desorption of some intermediate species such as $FeOH^+$ in reaction (4) above. The addition of either $LiNO_3$ or $CaCl_2$ modified this corrosion mechanism at the three different testing temperatures. Thus, at 25 and 50 °C, data displayed a single capacitive loop over all the testing frequencies, which is evidence that the corrosion process is under charge transfer control, and their addition increased the semicircle diameter obtained in the $LiBr+H_2O$ solution which increased in the following order: $CaCl_2$ > $LiNO_3$ > $CaCl_2$+$LiNO_3$ > $LiBr+H_2O$. At 80 °C, however, when these salts were added, a corrosion process

controlled by charge transfer and the diffusion of reactants was evident due to the presence of a capacitive loop at the highest frequency values followed by a straight line at tower frequencies in the Nyquist diagrams just as reported elsewhere [5, 31,39].

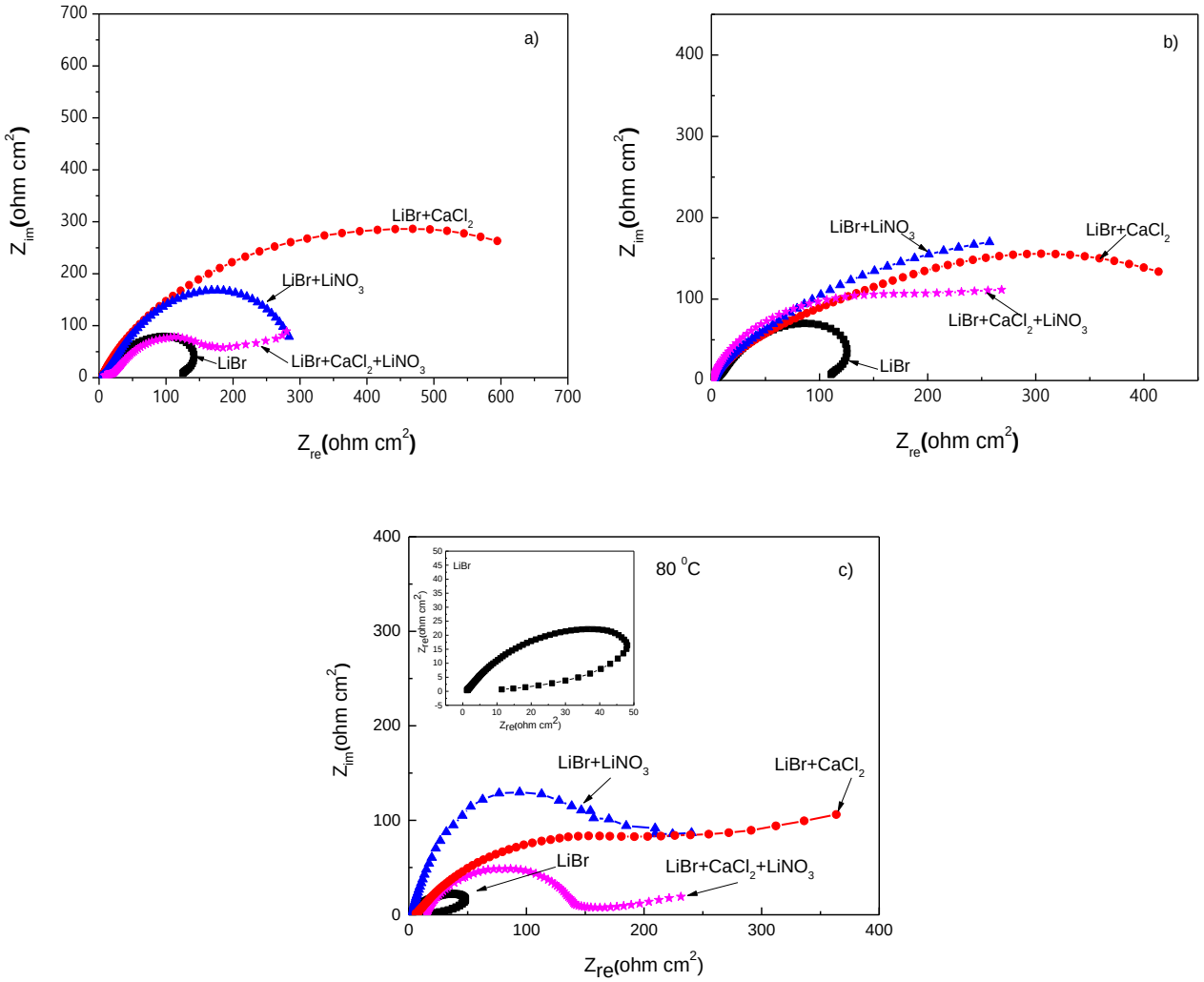

Figure 8. Effect of the addition of $CaCl_2$ and $LiNO_3$ to $LiBr/H_2O$ on the Nyquist diagrams for 1018 carbon steel at a LiBr concentration of a) 283.3, b) 425 and c) 850 g/L at 80 °C.

When the LiBr concentration was decreased, Fig. 8, the diffusion effect was kept only when both salts, i.e. $CaCl_2$+$LiNO_3$ were added in to the $LiBr+H_2O$ system. Nyquist diagrams obtained with the addition of either $CaCl_2$ or $LiNO_3$ displayed a single capacitive semicircle at all the frequency values, indicative of a charge transfer controlled corrosion process.

Thus, based on the obtained EIS results, three kind of equivalent electric circuits as those shown in Fig.9 can be used to simulate these results. The solution resistance are represented by R_s in Fig. 9, whereas the double layer properties such as charge transfer resistance and its capacitance are represented by R_{ct} and C_{dl} respectively, the corrosion products film properties such as resistance and capacitance are

R_f and C_f, and the Warburg impedance due to the reactants diffusion effect is represented by W, R_w its resistance, L the inductive element, R_L its resistance.

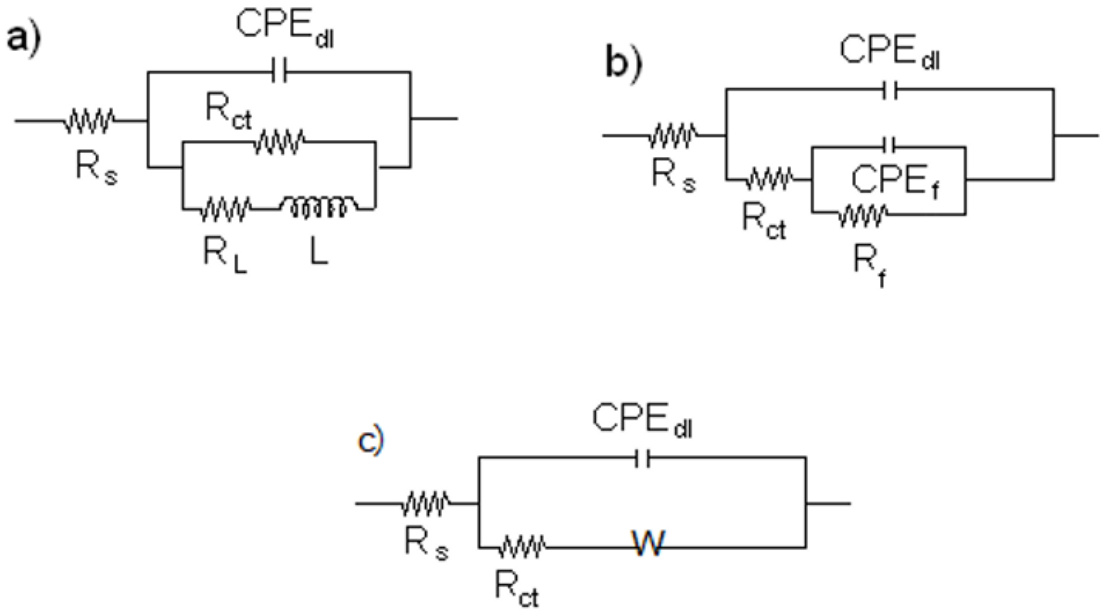

Figure 9. Electric circuits used to simulate EIS data for 1018 carbon steel immersed in a) LiBr+H_2O b) LiBr+H_2O+$CaCl_2$ or $LiNO_3$ at 25 and 50°C, and c) LiBr+H_2O+ $CaCl_2$ or $LiNO_3$ at 80°C.

Because the metal surface has some roughness due to its dissolution and to the presence of some heterogeneities, ideal capacitance is replaced by a constant phase element, CPE, which has an impedance, Z_{CPE}, given by:

$$Z_{CPE} = 1/[Y_0(i\omega)^n] \quad (7)$$

where Y_0 is a proportional factor and n has the meaning of a phase shift. When n = 0, CPE represents a resistance, when n = 1, a capacitance, when n = −1, an inductance, and when n = 0.5, a Warburg element, ω is the angular frequency (rad s−1), and i^2 is = −1 is an imaginary number. Resulting parameters from the use of circuits given in Fig. 9 for tests at different temperatures are shown in table 1.

This table shows that the R_{ct} values decreases as the testing temperature increases whereas the CPE_{dl} value increases due to an increase in the electrolyte aggressiveness as shown by the I_{corr} dependence on the temperature as given in Fig. 4. The lowest R_{ct} obtained values were for the LiBr+H_2O system, whereas the highest ones were obtained with the addition of $CaCl_2$, in agreement with results given by polarization curves, Fig. 3. The increase in the R_{ct} values with the addition of either $CaCl_2$, $LiNO_3$ or both is due to the formation of a much more compact passive layer and to an improvement in the steel corrosion resistance. The corrosion products film resistance, R_f, were lower than those for R_{ct}, and decreased as the testing temperature increased. On the other hand, the diffusion layer resistance, R_w, resulted in a maximum value when $CaCl_2$ was added, whereas the lowest value was obtained for the

addition of $CaCl_2$+$LiNO_3$. For the LiBr+H_2O system, the inductive element resistance value, R_L, decreased in a similar way as the other resistances values when the testing temperature increased.

Table 1. Electrochemical parameters used to fit EIS data for 1018 carbon steel in LiBr+H_2O containing $CaCl_2$ and $LiNO_3$.

Solution	Temp. (°C)	R_{ct} (ohm cm^2)	CPE_{dl} ($ohm^{-1}s^n$)	R_f (ohm cm^2)	CPE_f ($ohm^{-1}s^n$)	R_w (ohm cm^2)	R_L (ohm cm^2)
LiBr+H_2O	25	430	1.8×10^{-4}	-------	-------	-------	90
	50	190	5.0×10^{-4}	-------	-------	-------	68
	80	50	2.0×10^{-3}	-------	-------	-------	39
LiBr+H_2O +$CaCl_2$	25	900	3.3×10^{-4}	820	5.9 x10-4	-------	-------
	50	510	8.8×10^{-4}	230	1.0 x 10-3		
	80	205	1.6×10^{-3}	-------	-------	190	-------
LiBr+H_2O +$LiNO_3$	25	710	1.8×10^{-4}	300	9.1×10^{-4}	------	------
	50	530	4.7×10^{-4}	23	62		
	80	165	6.4×10^{-3}	-------	------	102	------
LiBr+H_2O +$CaCl_2$ +$LiNO_3$	25	525	3.3×10^{-4}	50	38	------	
	50	400	6.3×10^{-4}	20	25	------	------
	80	150	1.3×10^{-3}	-----	-------	75	------

3.4 Surface morphology analysis.

SEM micrographs of corroded specimens in the different systems at 25 and 80°C are shown in Figs. 10 and 11 respectively. It can be seen that, specimen corroded in the LiBr+H_2O system at 25°C, Fig. 10 a, surface morphology shows the presence of pits in combination with a generalized type of corrosion, but when $CaCl_2$ was added to the system, Fig. 10 b, surface morphology exhibits a very smooth surface, evidence that the damage due to the action of the electrolyte is very low in agreement with all the results given above. On the other side, specimen corroded in LiBr+H2O+ $LiNO_3$, Fig. 10 c, surface steel shows the absence of pits with a combination of uniform type of corrosion. Finally, for specimen corroded in LiBr+H_2O+ $CaCl_2$+$LiNO_3$, Fig. 10 d, some combination of some localized and uniform type of corrosion can be seen product of the localized attack produced by chloride ions and the passivation given by nitrate. For specimen corroded in the LiBr-H_2O system at 80°C, Fig. 11 a, a much rougher steel surface as compared with the test carried out at 25°C, Fig. 10 a, showing some uniform type of corrosion in combination with what looks like a localized type of corrosion but not precisely pits. On the other hand, specimen corroded in presence of $CaCl_2$, Fig. 11 b, shows a very smooth surface,

evidence that the damage done by the environment was very low, in combination with some pits. Specimen corroded in$LiBr+LiNO_3$, Fig. 11 c, shows a smooth surface in combination with a type of localized type of corrosion, very similar to that exhibited by the specimen corroded in presence of $CaCl_2$, Fig. 11 b. Finally, specimen corroded in $LiBr+CaCl_2+LiNO_3$, Fig. 11 d, surface morphology exhibited a combination of some localized and uniform type of corrosion just like the surface morphology fond for steel corroded in the same system but at 25°C, Fig. 10 d.

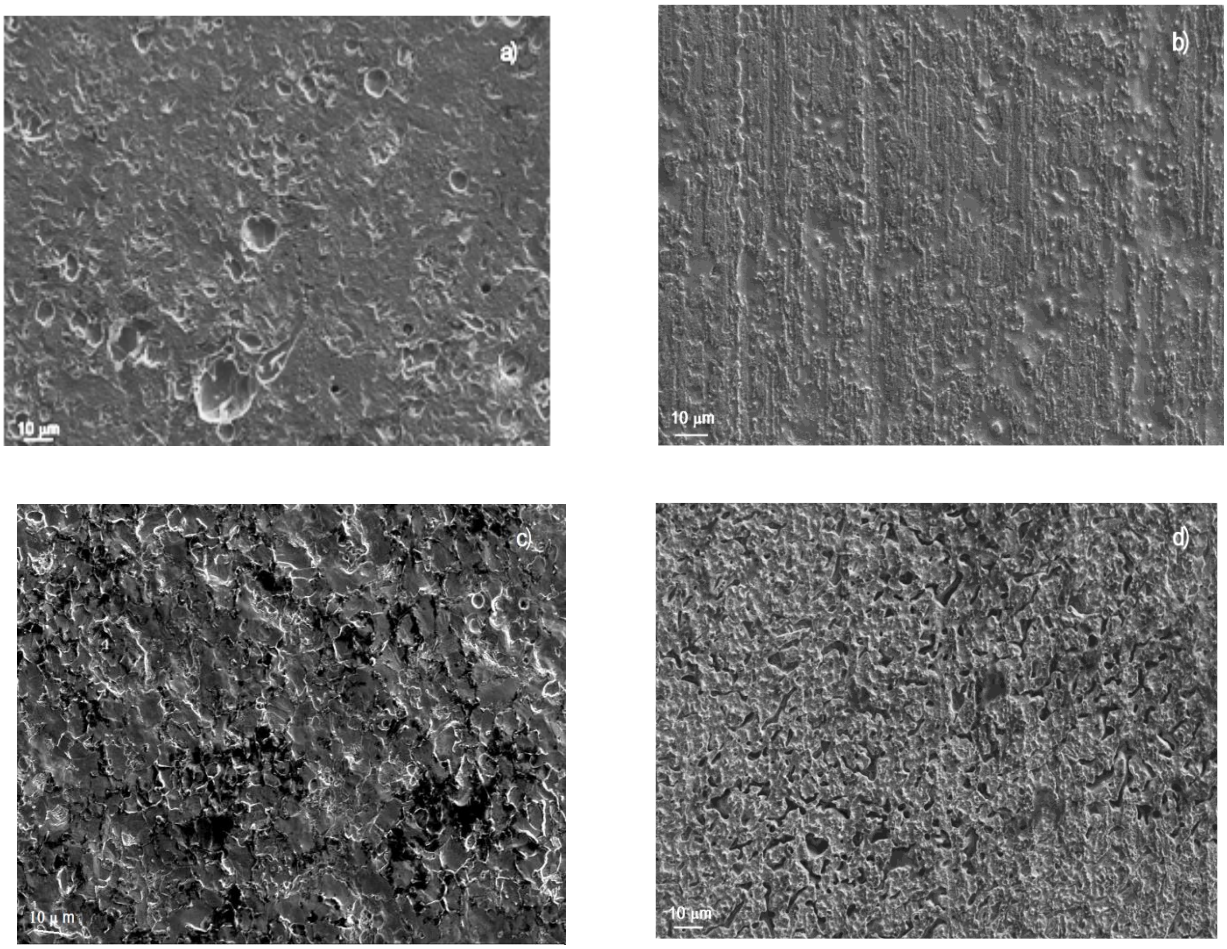

Figure 10. SEM micrographs of 1018 carbon steel corroded in a) $LiBr+H_2O$, b) $LiBr+H_2O+CaCl_2$, c) $LiBr+H_2O+LiNO_3$ and d) $LiBr+H_2O+CaCl_2+LiNO_3$ at 25°C.

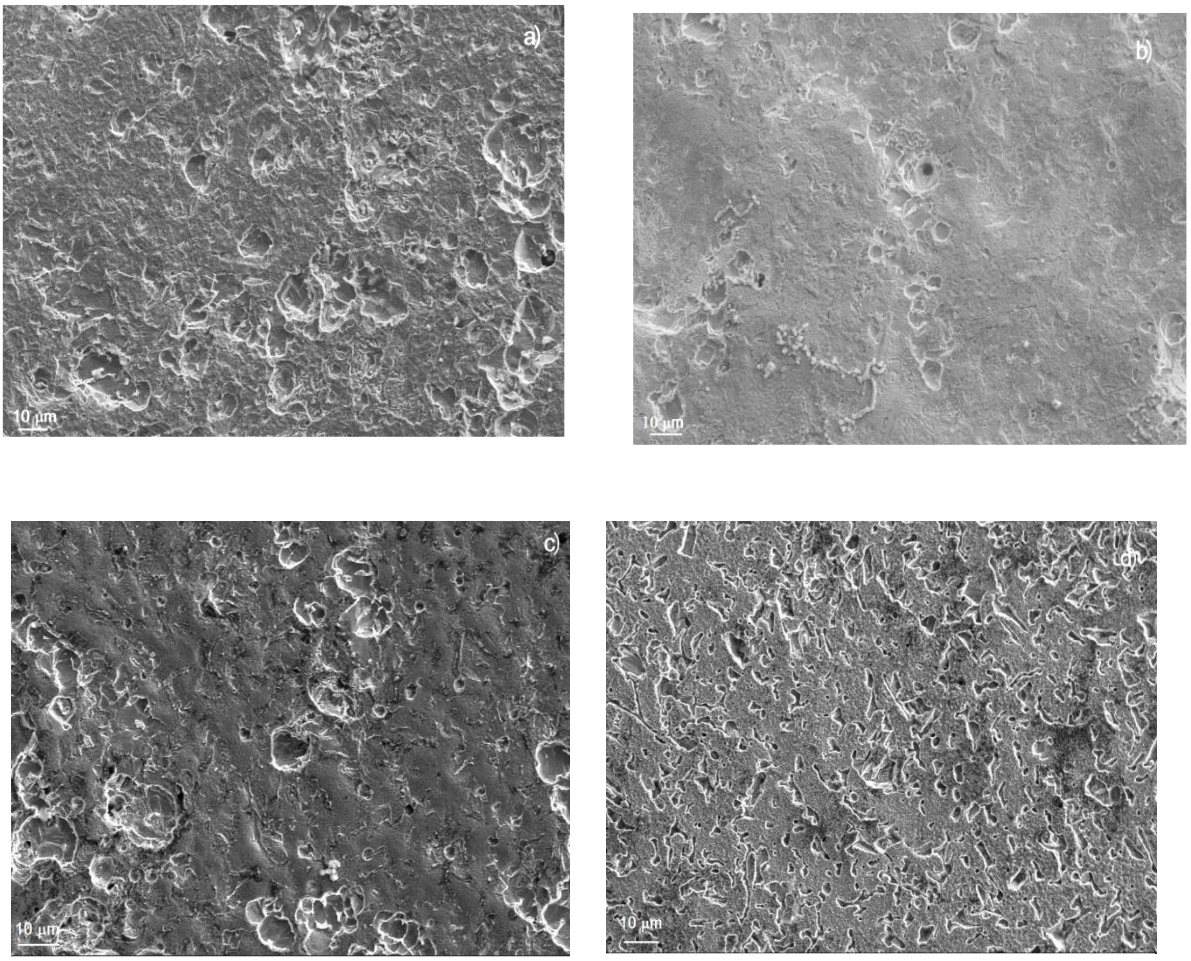

Figure 11. SEM micrographs of 1018 carbon steel corroded in a) LiBr+H_2O, b) LiBr+H_2O+$CaCl_2$, c) LiBr+H_2O+$LiNO_3$ and d) LiBr+H_2O +$CaCl_2$+$LiNO_3$ at 80°C.

4. CONCLUSIONS

Polarization curves have shown that the steel forms a passive layer on its surface in the LiBr-H_2O mixture which did not exist at the highest temperature, i.e. 80°C or at the highest concentration, i.e. 800 g/L. Instead, polarization curves with the addition of either $CaCl_2$, $LiNO_3$ or $CaCl_2$+$LiNO_3$ presented a passive layer at all temperatures or concentrations and reduced the I_{corr} value, which increased with the testing temperature and with the LiBr concentration. The I_{corr} value increased in the following order $CaCl_2$ < $CaCl_2$+$LiNO_3$ < $LiNO_3$ < LiBr+H_2O. Regardless the testing temperature or LiBr concentration, corrosion process in the LiBr+H_2O mixture was controlled by the adsorption/desorption of some intermediate species. On the other hand, corrosion process in the LiBr+H_2O mixture with the addition of either $CaCl_2$, $LiNO_3$ or $CaCl_2$+$LiNO_3$ was controlled by charge transfer at 25 and 50°C and under diffusion control at 80°C.

References

1. M. Deymi-Dashtebayaz, S. Maddah, M. Goodarzi, *J. Therm. Anal. Calorim.,* 141(2020)361.
2. M. Lickley, S. Solomon, S. Fletcher, G.J.M. Velders, J. Daniel, M. Rigby, S.A. Montzka, L.J.M. Kuijpers, K. Stone, *Nat Commun.,* 11(10)(2020)1380.
3. N. Mirl, F. Schmid, B. Bierling, K. Spindler, *Appl. Therm. Eng.,* 165(2020) 114531.
4. S.K. Lee, J.W. Lee, H. Lee, J.T. Chung, Y.T. Kang, *Energy,* 167(2019)47.
5. J. Hu, X. Xie, Y. *Int. J. Refrig.,* 118(2020)50.
6. A. Al-Falahi, F. Alobaid, B. Epple, *Case Stud. Therm. Eng.,* 22(3)(2020) 100763.
7. A. Mehari, Z.Y. Xu, R.Z. Wang, *Energy Convers. Manag.,* 206(2020)112482.
8. F. Cheng, Y. Li, X. Zhang, X. Li, *Appl. Therm. Eng.,* 172(2020)115130.
9. A.S. Alsagri, A.A. Alrobaian, S.A. Almohaimeed, *Energy Convers. Manag.,* 223(2020)113420.
10. M. Mosa, *Int. J. Air-Cond. Refrig.,* 27(5)(2019)1950026.
11. T. Inada, H. Tomita, F. Takemura, O. Tsubouchi, E. Hihara, *Int. J. Refrig.,* 100(2019)274.
12. S. Salehi, M. Yari, S.M.S. Mahmoudi, L. Garousi-Farshi, *Therm.Sci. Eng. Prog.,* 10(1)(2019)48.
13. K.L. Cézar, A.G.A. Caldas, A.M.A. Caldas-Cordeiro, M.C.L. Dos Santos, A.A.V. Ochoa, P.S.A. Michima, *Int. J. Refrig.,* 111(2020)124.
14. Y. Cho, S. Han, H. Seo, M. Shin, S. Woo, S.Jeong, *J. Mech. Sci. Technol.,* 33(10)(2019) 2995.
15. J. Yoo, S. Han, Y. Nam, S. Jeong, *J. Mech. Sci. Technol.,* 34(9)(2020) 4037.
16. E.A. Abd El Meguid, S.S. Abd El Rehim, S.A. Al Kiey, *Corros. Eng. Sci. Technol.,* 51(3)(2016) 429.
17. S. Zolfaghari, A.R. Baboukani, A. Ashrafi, A. Saatchi, *Zastita Materijala,* 59(1)(2018)108.
18. V. Guiñón-Pina, A. Igual-Muñoz, J. García-Antón, *Int. J. Electrochem. Sci.,* 6(9)(2011) 6123.
19. G.I. Youssef, A.E. El Meleigy, L.A. Khorshed, A. Attia, E.A. Ashour, *Mater. Corros.,* 69(6)(2018)1827.
20. S.A. Elhamid, A.E. Meleigy, A. Attia, A.E. Warraky, S. Abd-El-Wahab, *Egypt. J. Chem.,* 63(4)(2020) 907.
21. N. Li, C. Luo, Q. Su, *Int. J. Refrig.,* 86(2018) 1.
22. Y. Li, N. Li, C. Luo, Q. Su, *Entropy,* 21(3)(2019) 546.
23. T. Torres-Díaz, J. Siqueiros, A. Coronas, D. A. Salavera Huicochea, D. Juárez-Romero, *Desalin. Water Treat.,* 82(2017) 292.
24. E. Bellos, C. Tzivanidis, S. Pavlovic, V. Stefanovic, *Therm. Sci. Eng. Prog.,* 3(1)(2017) 75.
25. C. Luo, Q. Su, N. Li, Y. Li, *Int. J. Electrochem. Sci.,* 12(3)(2017) 1896.
26. D. Yang, Y. Zhu, S. Liu, H. Lu, C Luo, C. *J. Chem. Eng. Data,* 64(4)(2019) 574.
27. S.M. Osta-Omar, C. Micallef, *Data,* 2(1)(2017) 6.
28. S. Jian, F. Lin, Z. Shigang, Z. *Appl. Therm. Eng.,* 30(8)(2010) 2680.
29. J. Guo, C. Liang, *Corros. Eng. Sci. Technol*., 14(2)(2002) 197.
30. [30] K. Rahmouni, M. Keddam,A. Srhiri, H. Takenouti, *Corros. Sci.* 2005*,* 47, 3249.
31. C.H. Liang, X.Q. Hu, L. Ma*, Mater. Corr*. 58(1)(2007) 39.
32. X. Q. Hu, C. H. Liang, X. N. Wu, *Mater. Corr*. 62(3)(2011) 444.
33. E. Samiento-Bustos, J.G. González Rodriguez, J. Uruchurtu, G. Dominguez-Patiño, V.M. Salinas-Bravo, *Corros. Sci.,* 50(10)(2008) 2296.
34. S.J. Ren, J. Charles, X.C. Wang, F.X. Nie, C. Romero ,S. Neti, Y. Zheng, S. Hoenig, C. Chen, F. Cao, R. Bonner, H. Pearlman, *Mater. Corros*., 68(1)(2017) 1.
35. J.C. Estill, G.A. Hust, K J. Evans, M.L. Stuart, R. B. Rebak, presented at ASME Pressure Vessels and Piping Division Conference, Vancouver, Canada, July 23-27, (2006)1.
36. M. Itoh, K. Itoh, M. Izumiya, K. Tanno, *Boshoku Gijutsu,* 38(3)(1989) 645.
37. C.A.C. Sequeira, *High Temperature Corrosion: Fundamentals and Engineering,* Wiley-Blackwell. London, 2019.
38. J.L. Guiñon, J. Garcia-Anton, V. Pérez-Herranz, G. Lacoste, Corrosion 50(1)(1994) 240.

39. J. Li, C. Liang, N. Huang, *J. Mater. Eng. Perf*., 24(12)(2015) 4456.